Geophysical Research Letters

RESEARCH LETTER
10.1029/2022GL099476

Present-Day Upper-Mantle Architecture of the Alps: Insights From Data-Driven Dynamic Modeling

Ajay Kumar[1], Mauro Cacace[1], Magdalena Scheck-Wenderoth[1,2], Hans-Jürgen Götze[3], and Boris J. P. Kaus[4]

[1]GFZ, German Research Centre for Geosciences, Potsdam, Germany, [2]Faculty of Georesources and Materials Engineering, RWTH Aachen University, Aachen, Germany, [3]Institute of Geosciences, Christian-Albrechts-University of Kiel, Kiel, Germany, [4]Institute of Geosciences, Johannes Gutenberg University of Mainz, Mainz, Germany

Abstract The dynamics of the Alps and surrounding regions is still not completely understood, partly because of a non-unique interpretation of its upper-mantle architecture. In particular, it is unclear if interpreted slabs are consistent with the observed surface deformation and topography. We derive three end-member scenarios of lithospheric thickness and slab geometries by clustering available shear-wave tomography models into a statistical ensemble. We use these scenarios as input for geodynamic simulations and compare modeled topography, surface velocities and mantle flow to observations. We found that a slab detached beneath the Alps, but attached beneath the Northern Apennines captures first-order patterns in topography and vertical surface velocities and can provide a causative explanation for the observed seismicity.

Plain Language Summary Present-day surface deformation, including earthquakes, plate motion, and mass (re)distribution, results from processes operating at the surface and in the interior of the Earth. Understanding these processes and their coupling is of utmost importance in light of the hazard they pose to society. The Alps provide an excellent natural laboratory to understand such coupling. Here, we use seismic tomography models to constrain its upper-mantle architecture. We further use these models to quantify forces originating from the resolved architecture and their effects on the present-day surface deformation. The models can reproduce first-order patterns in the observed topography and vertical surface motions. We found a causative correlation between the presence of a shallow slab attached to the overlying lithosphere in the Northern Apennines and the seismicity in the region. Our results allow us to better understand the transfer of internal forces to the surface, thereby helping to quantify the present-day mechanical setup of the area.

Key Points:

- Statistical ensemble of S-wave tomography models is used to infer the Lithosphere-Asthenosphere Boundary configuration and slab geometries in the Alps
- The 3-D upper-mantle architecture from the statistics reproduce first-order patterns in observed topography and Global Navigation Satellite Systems vertical velocities
- A shallow/attached slab in the Northern Apennines is consistent with the mantle depth seismicity observed in this region

Supporting Information:

Supporting Information may be found in the online version of this article.

Correspondence to:

A. Kumar,
kumar@gfz-potsdam.de

Citation:

Kumar, A., Cacace, M., Scheck-Wenderoth, M., Götze, H.-J., & Kaus, B. J. P. (2022). Present-day upper-mantle architecture of the Alps: Insights from data-driven dynamic modeling. *Geophysical Research Letters*, *49*, e2022GL099476. https://doi.org/10.1029/2022GL099476

Received 11 MAY 2022
Accepted 1 SEP 2022

1. Introduction

Geodetic observations by the Global Navigation Satellite Systems (GNSS) show that the Alpine mountains are uplifting while their forelands to the north and south are subsiding (Figure 1, Serpelloni et al., 2022; Sternai et al., 2014). Vertical uplift also varies along strike, with higher rates in the Western and Central Alps (~2–2.5 mm/yr) than in the Eastern Alps, similar to inferred erosion and exhumation rates (Fox et al., 2015). Horizontal velocities from GNSS show ~2 mm/yr convergence between Adria and Europe in the Eastern Alps, being related to the counter-clockwise rotation of the Adria microplate with respect to Eurasia, while convergence is only minor, if not absent, in the Western Alps (Serpelloni et al., 2016). Seismicity is restricted to upper-crustal depths in the Alps compared to whole crustal seismicity in their forelands (Figure 1). Earthquakes below Moho (>40 km) occur only to the south, beneath the Northern Apennines. A combination of surface and/or mantle processes have been proposed to explain these observations, including: (a) isostatic response to the latest deglaciation, (b) long-term erosion, (c) crustal shortening, (d) delamination of the European lithosphere, (e) detachment of the Western Alpine slab, and, (f) mantle flow in the asthenosphere (Fox et al., 2015; Mey et al., 2016; Sternai et al., 2014). Quantifying the relative contribution of these processes to the present-day surface deformation is essential to understand the coupling between surface and mantle processes and the evolution of this complex orogen.

Mey et al. (2016) proposed that ~90% of rock uplift in the Alps could be due to crustal rebound following the Last Glacial Maximum, while mantle processes exert only a local influence (e.g., Rhone Valley and Eastern Alps). Recently, Sternai et al. (2019) critically revisited this hypothesis. They demonstrated how deglaciation and erosion account for a relatively larger proportion of uplift in the Eastern Alps (30%–60%) than in the Central

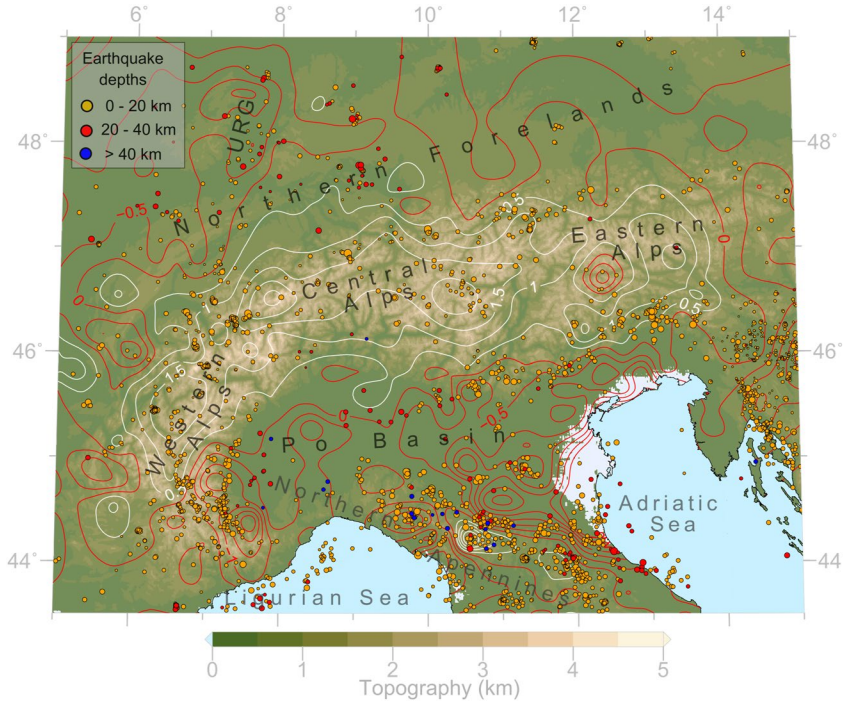

Figure 1. Topography map showing surface uplift (solid lines) and seismicity (circles), scaled by magnitude (M_{Lv}: 0.4–4.9) and color-coded by depth, taken from the AlpArray Research Seismiciy-Catalog (Bagagli et al., 2022) in the Alps and surrounding regions. Vertical velocities from Global Navigation Satellite Systems measurements (Sternai et al., 2019) are interpolated and contoured at a 0.5 mm/yr interval; white contours represent uplift, and red represents subsidence. Note that the 0 mm/yr contour is plotted in red.

and Western Alps (20%–30%), and attributed the remaining uplift to other tectonic processes. This speculative contribution from tectonic processes stems from uncertainties in the upper-mantle (i.e., lithospheric mantle and asthenosphere) architecture. A thicker crust beneath the Alps with intermediate average densities has been shown to correlate with observed surface uplift (Spooner et al., 2019a). Beneath the Alps, upper-crustal seismicity (Cattaneo et al., 1999; Eva et al., 2015; Singer et al., 2014) occurs within a weaker orogenic lithosphere, while weaker crustal domains are found preferentially around the stronger Adriatic microplate in the southern foreland (Marotta & Splendore, 2014; Spooner et al., 2022; Willingshofer & Cloetingh, 2003). In the northern forelands, the entirety of crustal seismicity (Deichmann, 1992; Singer et al., 2014) is also bound to weaker crustal areas, which underwent extensive thinning beneath the Upper Rhine Graben.

These correlations indicate the importance of lithospheric architecture in the localization of surface deformation within the Alpine region. However, the causality of these correlations remains subject to a proper quantification of the active driving forces. Forces within the Alpine lithosphere arise from horizontal plate motions, potential energy gradients due to present-day topography and lateral variations in density, and variations in surface loading. Negative buoyancy from subducted lithospheric slabs within a weaker asthenosphere can generate flow and, therefore, stresses within and along the base of the lithosphere. Hence, to quantify these forces and understand their contribution to the present-day surface deformation, it is crucial to determine the present-day 3-D upper-mantle architecture.

Seismic tomography provides information to unravel the architecture of the upper-mantle. However, interpretation of these models is non-unique (e.g., Foulger et al., 2013). For example, a recent interpretation of P-wave travel time tomography (Handy et al., 2021; Paffrath et al., 2021) suggests presence of an European slab detached below the Western and Eastern Alps being locally attached to the lithosphere in the western Central Alps. In contrast, a surface-wave dispersion tomography model (El-Sharkawy et al., 2020) is consistent with slabs attached below most of the Central Alps. Kästle et al. (2020) compared all available regional high-resolution body-wave tomography models and concluded that slabs below the Alps differ significantly in their shapes and lengths. Such differences in the tomography interpretation arise from the choice of the reference model adopted, and the

relative velocity contrasts used to define velocity anomalies. Recent developments in the field of mineral physics and availability of updated laboratory-derived pressure and temperature-dependent elastic properties can help to infer seismic velocities in terms of temperature and/or composition, thus providing a quantitative way to interpret tomography models (e.g., Cammarano et al., 2003; Goes et al., 2000; Priestley & McKenzie, 2006).

In this work, we use these additional constraints to determine present-day upper-mantle architecture of the Alps and their forelands from available tomography models. We convert these models to temperature models to objectively determine topography of the Lithosphere-Asthenosphere Boundary (LAB) and geometry of slabs in the asthenosphere. These models are then used to compute the contribution to present-day deformation from buoyancy forces arising from the input configuration to add physical constraints to present-day upper-mantle architecture.

2. Methods and Data

2.1. Crust

The thickness of the crustal layers in the Alps and surrounding regions is integrated from a 3-D crustal model by Spooner et al. (2019a). In our study, we extend the model laterally to reduce potential boundary effects for the later geodynamic modeling stage by complementing it with EuCrust-07 model (Tesauro et al., 2008), Figures 2a–2c.

2.2. Upper-Mantle

Shear-wave velocities (Vs) are more sensitive to variations in temperature than variations in composition (Kumar et al., 2020; Priestley & McKenzie, 2006). Thus, we use Vs tomography to map the temperature distribution in the mantle. We rely on four Vs tomography models, viz. CSEM (Fichtner et al., 2013, 2018), EU60 (Zhu et al., 2015), MeRe2020 (El-Sharkawy et al., 2020), and SL2013 (Schaeffer & Lebedev, 2013). To account for varying spatial resolutions of these models, we interpolated them to a common grid size of 20 × 20 km horizontally and 5 km in-depth, from 50 to 300 km depth.

Conversion of seismic velocities to temperatures is highly non-linear because of the pressure and temperature dependence of elastic moduli, anelasticity, and/or the presence of partial melts (Figure S1 in Supporting Information S1). To overcome this non-linearity, we pre-compute anharmonic Vs from stable phase and mineral assemblages at upper-mantle pressure and temperature conditions. Stable phase and mineral assemblages are derived using a Gibbs free-energy minimization algorithm (Connolly, 2005, 2009). We use the augmented-modified version of Holland and Powell, 1998 thermodynamic database (Afonso et al., 2008; Afonso & Zlotnik, 2011) and depleted-mid-oceanic-ridge-basalt-mantle (DMM, Workman & Hart, 2005) as bulk composition. Pressure and temperature-dependent anharmonic Vs are corrected for anelasticity and effects of partial melts using the parameters derived from laboratory experiments on olivine polycrystalline rocks (Jackson & Faul, 2010) and empirical relations for dry-peridotite solidus and liquidus (Afonso et al., 2016; Hammond & Humphreys, 2000; Hirschmann, 2000; Winter 2010), respectively (Text S1 in Supporting Information S1).

The absolute Vs values from the tomography models are then projected onto the pre-computed look-up table of Vs using a lithostatic pressure profile derived from a thermo-chemical equivalent model of ak135 (Kennett & Engdahl, 1991; Kumar et al., 2020), thus providing a 3-D distribution of temperature in the upper-mantle. We use a thermal definition of the LAB with a threshold temperature of 1300°C as characteristic for the solidus of peridotite intersecting an average geotherm (Hirschmann, 2000). We use the 1300°C isotherm to differentiate between lithospheric mantle, slabs, and asthenosphere. Regions corresponding to temperatures >1300°C are defined as ambient asthenosphere. To distinguish between the lithospheric mantle and subducted slabs in the asthenosphere, we opted for a cut-off depth of 200 km; that is, if the 1300°C isotherm lies above (below) this depth, then the portion of the mantle that is colder than 1300°C is taken as lithospheric mantle (subducted slabs). The choice of this reference depth is justified by the observation that the Phanerozoic European lithosphere (LAB depth ∼120 km, Griffin et al., 2009) can be as thick as 200 km beneath the Alps (Artemieva, 2019) and the minimum of the reported slab break-off depths in analog and numerical experiments (Fernández-García et al., 2019).

2.3. Buoyancy-Driven Dynamic Flow

To compute the deformation in response to the first-order internal thermomechanical configuration, we solve the conservation of momentum and mass equations to calculate stresses, velocities, and topography using LaMEM

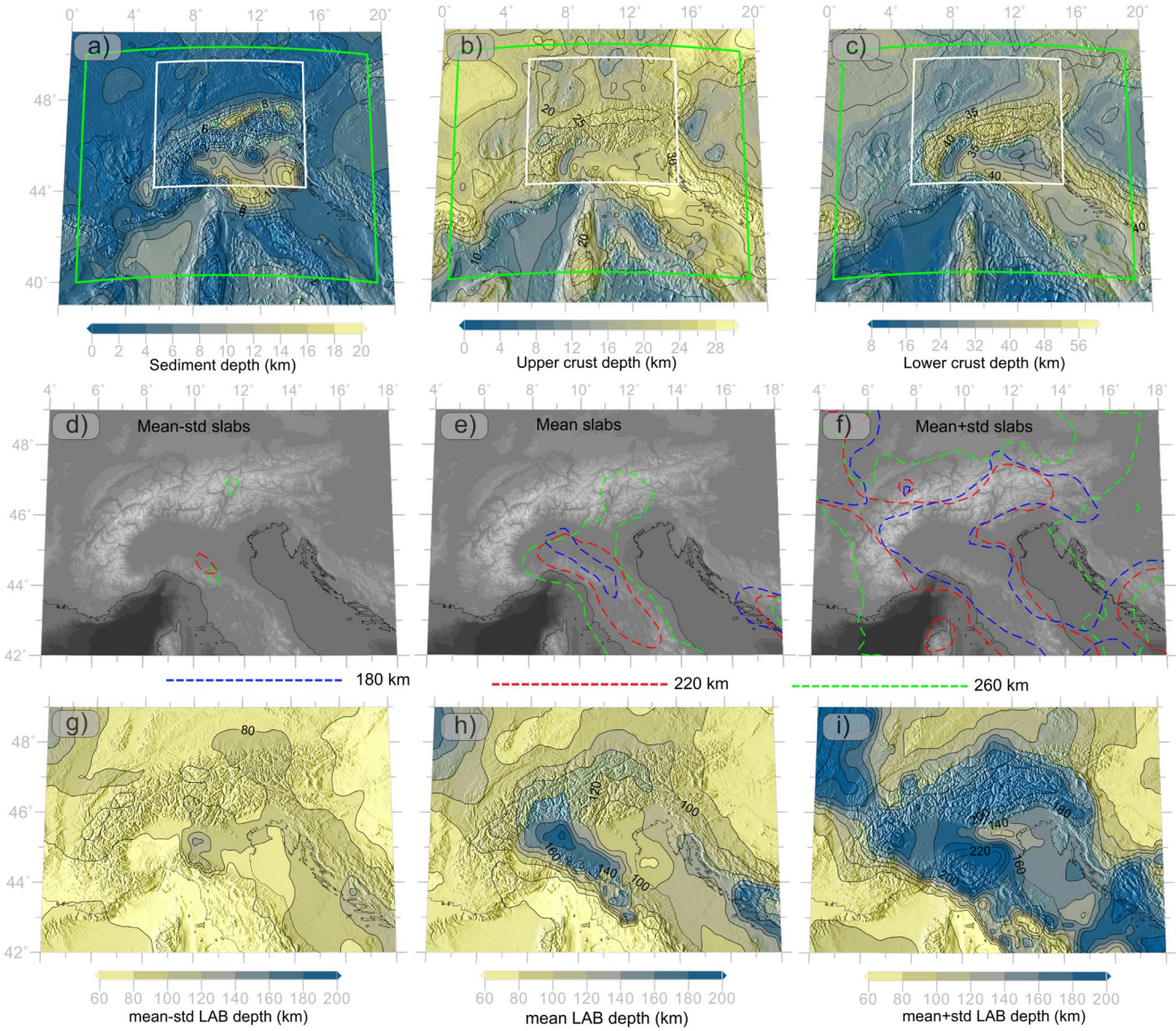

Figure 2. Depth of the (a) sediments, (b) upper-crust, and (c) lower-crust. The white box in each panel marks the extent of the gravity-constrained 3-D crustal model, and the green box shows the extent of the region modeled in this study. Geometries of the slabs (d–f) and Lithosphere-Asthenosphere Boundary depths (g–i) for the statistical ensemble of tomography models. Color-coded dashed contours in panels (d–f) delineate the slabs at 180, 220, and 260 km depths.

(Text S2 in Supporting Information S1). The modeling domain is a 3-D Cartesian box with 96 × 96 × 128 grid points giving a resolution of ∼13 km in E-W, ∼17 km in N-S, and ∼3 km along depth. Thicknesses of the crustal layers with respect to the digital elevation model, ETOPO1 (Amante & Eakins, 2009), are used such that the initial internal free-surface (Crameri et al., 2012; Kaus et al., 2010) is flat at 0 km. We consider a first-order rheological structure where the lithosphere (i.e., sediments, upper-crust, lower-crust and lithospheric mantle) and slabs are stronger than the asthenosphere (Table 1). Slabs are considered to be 70 kg/m^3 denser than the asthenosphere (Table 1). We also test the sensitivity of results to variations in viscosity and density contrasts between the lithospheric mantle, slabs, and asthenosphere (Text S4 in Supporting Information S1). To investigate the dynamic effects of the internal buoyancy related to the upper-mantle configuration, we allow all models to obtain isostatic balance until a quasi-isostatic equilibrium is achieved (∼0.27 Ma, Figure S2 in Supporting Information S1) and a return flow is fully established without significantly deforming the slabs from their initial geometry (Figures 2 and 3).

Table 1
Physical Properties of the Layers in the Dynamic Models

Layer/Phase	Density (kg/m^3)	Viscosity (Pa.s)
Sticky-air	1	10^{18}
Sediments	2,450	10^{22}
Upper-crust	2,750	
Lower-crust	2,950	
Lithospheric mantle	3,370	
Slabs	3,370	
Asthenosphere	3,300	10^{20}

Note. Densities in the crust are according to Spooner et al. (2019a). Density and viscosities in the lithosphere, slabs, and asthenosphere are according to Boonma et al. (2019), Mey et al. (2016), Sternai et al. (2019), and Spooner et al. (2022).

3. Results

3.1. Upper-Mantle Architecture

The geometry and depth extent of the slabs from each tomography model share similarities in the Northern Apennines but differ significantly in the Alps (Figure S4 in Supporting Information S1). All regional tomography models (CSEM, EU60 and MeRe2020) depict an attached slab in the Northern Apennines with varying volume and position. In SL2013, a shallow slab is present from beneath the Northern Apennines to the Alps in north. EU60 indicates an attached slab all along the Eastern Alps, which is connected to attached slabs in the Western Alps and Northern Apennines. CSEM displays an attached slab at the Western and Central Alps transition, similar to the interpretation of a recent P-wave tomography model (Handy et al., 2021). MeRe2020 shows a locally attached slab to the lithosphere in the Central Alps.

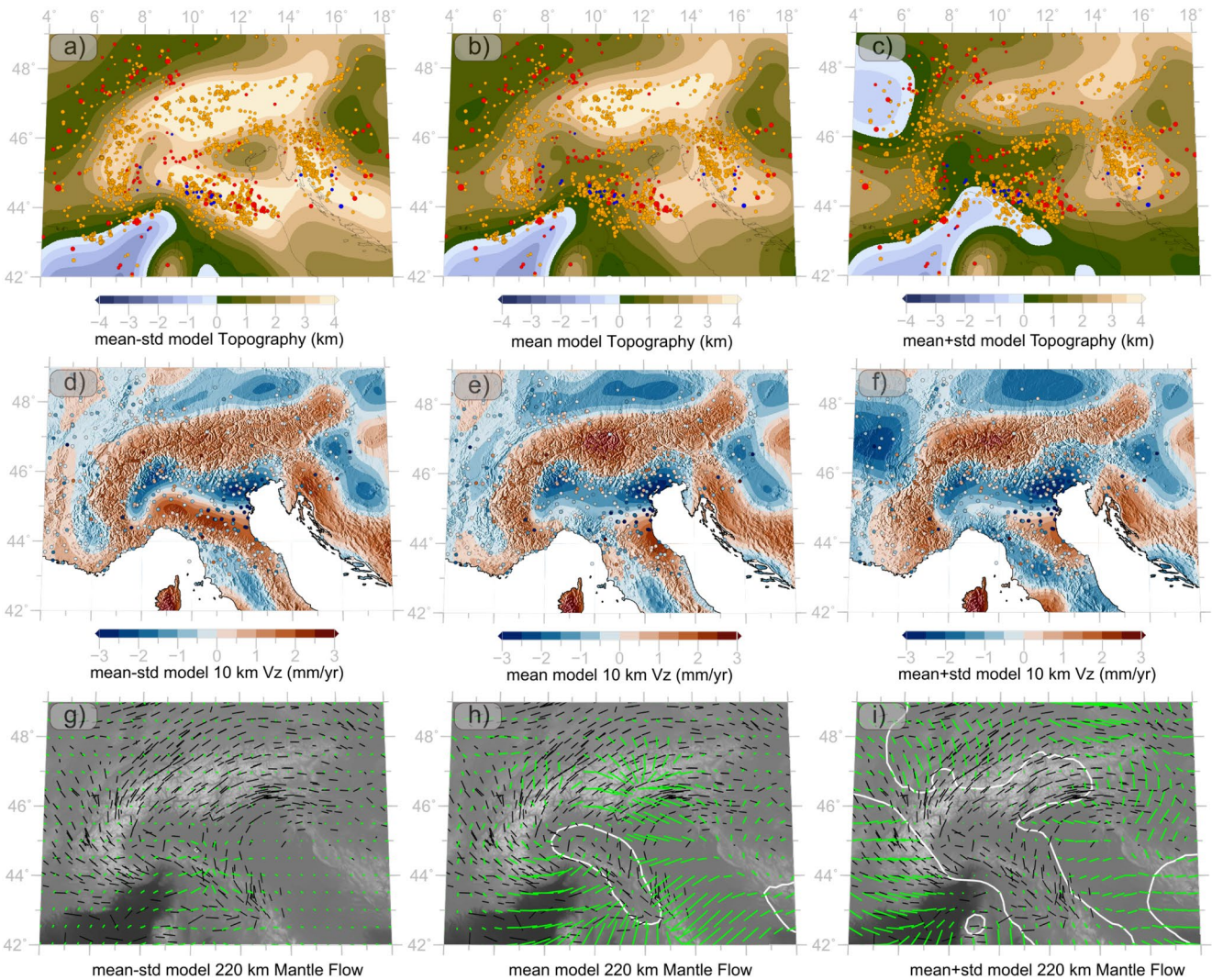

Figure 3. Modeled topography for (a) mean-std, (b) mean, and (c) mean+std models. Seismicity color-coded for depth is same as in Figure 1. Vertical velocities at 10 km depth for (d) mean-std, (e) mean, and (f) mean+std models with Global Navigation Satellite Systems measurements plotted with circles. Horizontal flow in the asthenosphere at a depth of 220 km for (g) mean-std, (h) mean, and (i) mean+std models are plotted as green lines scaled by velocity magnitude. Shear-wave splitting measurements scaled by the delay time are plotted with black bars (Hein et al., 2021). White lines in the last three panels indicate the contour of the slabs at 220 km depth.

Differences in slab geometries stem from the fact that the tomography models have varying resolution, and magnitudes and spatial distributions of Vs (Figure S5 in Supporting Information S1). Consequently, converted temperatures differ, making it challenging to define a unique architecture of the LAB and slabs (Figures S4 and S5 in Supporting Information S1). Further, different methods, data and regularizations used in the inversion cause model-specific uncertainties. To objectively address such differences in the tomography models, we cluster them into a statistical ensemble, thereby assuming that these models sample a range of possible solutions though with a variable resolution. The statistical ensemble corresponds to the mean and standard deviation (std) of Vs from all tomography models at each grid point. The mean of Vs is clustered into a model (mean model hereafter), whereas Vs corresponding to the 67% confidence interval are clustered into two additional models (mean-std and mean+std hereafter). The mean-std model represents an end-member scenario featuring no slabs beneath the Alps and Northern Apennines (Figure 2d). The mean+std model is an end-member at the opposite spectrum where slabs are attached to the overlying lithosphere below the Alps and Northern Apennines (Figure 2f). In the mean model, a slab is only attached to the overlying lithosphere beneath the Northern Apennines (Figure 2e).

Each model also shows a varying LAB depth (Figures 2g–2i). All models show a thin lithosphere (~60–80 km) in the Ligurian Sea and Pannonian Basin. The mean-std model results in a thinner lithosphere in the Alps and Northern Apennines. In the mean and mean+std models, LAB depth is controlled by the presence of the slabs. Therefore, the mean+std model results in the thickest lithosphere beneath the Alps, Po Basin, and Northern Apennines, where slabs are envisaged as attached to the lithosphere (Figure 2i). The presence of a thinner lithosphere in the northern forelands compared to the orogenic lithosphere in the Alps is a common feature of both the mean and mean+std models. In the following, we present results of the geodynamic simulations for the statistical ensemble models. Simulations have also been carried out for the individual tomography models for comparison (Text S3 in Supporting Information S1).

3.2. Topography

In the absence of far-field tectonic forces, modeled topography is a function of the crust and lithosphere thickness and geometry of the slabs, attached to or detached from the orogenic lithosphere. For the mean-std model, where no slabs are attached to the lithosphere, and the lithosphere is overly thin, the modeled topography reflects resolved crustal thickness variations (Figures 2c and 3a). It results in a negative topography along the present-day coastline in the Ligurian Sea and a positive topography in the Alps (~3–4 km), higher than in the northern forelands and Pannonian Basin. Along strike variations in crustal thickness in the Alps are also reflected in the modeled topography, being lower above the thinner crust in the Western Alps than in the Central and Eastern Alps. In the Northern Apennines, the model displays topography of similar magnitudes as in the Alps, which is inconsistent with observations (Figure 1). The negative residual topography along the Alps and Northern Apennines for the mean-std model is indicative that crustal isostasy alone is not enough to explain the observed topography (Figure S8 in Supporting Information S1). Despite similar magnitudes of crustal thickness beneath the Adriatic Sea and northern forelands (Figure 2c), the mean-std model produces positive topography all along the Northern Apennines to Dinarides. The mean model features a lower topography in the Alps compared to the mean-std, still higher than that obtained in both forelands (Figure 3b). The lower topography in the Northern Apennines and Po Basin than the one obtained from the mean-std model can be explained by an attached slab in the Northern Apennines, which effectively pulls down the overlying lithosphere (Figure S3a in Supporting Information S1). This gravitational effect is enhanced in the mean+std model (Figure 3c and Figure S3b in Supporting Information S1) and it does not produce any elevation gradient between the Alps and their forelands. Relatively high topography in the Adriatic Sea persists in the mean+std model, though of lower magnitudes due to a thicker lithosphere (Figure 2i).

3.3. Surface Vertical Velocities

Geometries of the slabs also affect modeled vertical velocities. The mean-std model produces uplift in the Alps and subsidence in the northern and southern forelands (Figure 3d). Subsidence in the Po Basin is limited by uplift in the Northern Apennines. In contrast, in the mean model, subsidence in the Po Basin continues to the south into the Northern Apennines consistent with the observations (Figure 3e and Figure S3c in Supporting Information S1). The mean model also produces higher uplift in the Central Alps compared to the Western and Eastern Alps. The mean+std model, where slabs are attached all along the Alps and Northern Apennines, cannot

reproduce the observed uplift in the Alps. Attached slabs to the thicker lithosphere lead instead to overall subsidence in the Po Basin, which continues to the north into southern half of the Alps and to south into the Northern Apennines (Figure 3f and Figure S3d in Supporting Information S1).

3.4. Mantle Flow

Horizontal flow in the asthenosphere also shows differences in pattern and magnitude for the three scenarios (Figures 3g–3i). The mean-std model shows a less vigorous mantle flow than the mean and mean+std models due to the absence of slabs. In the mean model, we observe a rotation in mantle flow around the Western Alps due to a return flow generated by the attached slab in the Northern Apennines. This is consistent with shear-wave splitting (SKS) measurements that also show a rotation of the fast axis around the Western Alps (Figure 3, Barruol et al., 2011; Hein et al., 2021). In the mean+std model, such a rotation is hindered by the presence of an attached slab beneath the Alps. In the Central and Eastern Alps, the mean model displays an orogen-subparallel flow, which is not as coherent as observed in SKS measurements. However, the mean model does reproduce the rotation in mantle flow at the transition from the Eastern Alps toward the Pannonian Basin, as observed in SKS measurements.

4. Discussion and Summary

4.1. Upper-Mantle Architecture

Active subduction of an attached oceanic lithosphere is manifested in deep seismicity delineating the classical Benioff-Wadati zone. If the subducting lithosphere is tearing or breaking-off, it might show a concentration of intermediate-depth seismicity. Such a process is thought to be occurring in the Vrancea zone in the SE-Carpathians, where we observe a concentration of intermediate-depth seismicity and a positive seismic velocity anomaly (Wenzel et al., 2002). In Southern Iberia, a slab beneath the Betics mountains is also considered to be tearing/detaching, leading to the observed seismicity clustering (e.g., Heit et al., 2017; Mancilla et al., 2015). The preferred model for the slabs beneath the Alps portrays a detached slab in the Western Alps (El-Sharkawy et al., 2020; Handy et al., 2021; Kästle et al., 2020; Lippitsch et al., 2003). In the Eastern Alps, the majority of models agree with a detached slab; however, there is an ongoing discussion on its maximum depth, dip and association, whether Adriatic or European (Handy et al., 2021; Lippitsch et al., 2003). In the western Central Alps, a recent publication (Handy et al., 2021) indicated the possible presence of an attached slab to depths >300 km, in contrast to the conclusions by Lippitsch et al. (2003). Lower-crustal seismicity in the European crust to north of the Central Alps is interpreted to be driven by transfer of stresses to the northern forelands from a retreating European slab after slab break-off (Kissling & Schlunegger, 2018; Singer et al., 2014) or by the presence of high-pressure fluids in the lower-crust (Deichmann, 1992). Additionally, the absence of lower-crustal and intermediate-depth seismicity in the Alps could be related to detached slabs all along the Alps as represented by the mean and mean-std models or by slow convergence in the Alps (Dal Zilio et al., 2018). An attached slab beneath the Central Alps implies seismic deformation at lower-crustal depths or even at upper-mantle depths. Seismicity in the Alps is shown to be effectively bounded by 450°C isotherm within the upper-crust (Spooner et al., 2020). These observations suggest a detached slabs model, which can explain only upper-crustal seismicity beneath the Alps. However, the modeled lower topography in the Western Alps would require additional variations in the present-day load along the Alps to either increase topography in the Western Alps or decrease it in the Central and Eastern Alps, for example, mean+std model. Alternatively, rebound from recent slab break-off could have uplifted/uplifting the Western Alps and moved them out of isostatic equilibrium. High erosion rates in this domain compared to the Eastern Alps can be then interpreted as consequence of a system still achieving isostatic equilibrium (Fox et al., 2015). We can, therefore, not rule out this working hypothesis with our study.

An attached shallow slab in the Northern Apennines is a robust feature in all regional tomography models. Our results suggest that such a configuration is also required to reproduce the present-day observed lower topography and widespread subsidence rates in the Po Basin and Northern Apennines compared to the Alps (Figure 1 and Figure S8 in Supporting Information S1). An attached slab is also consistent with the observed mantle seismicity (e.g., Chiarabba et al., 2005), with earthquakes occurring at depths where we would otherwise expect rocks to behave aseismically.

4.2. Geodynamic Implications

None of the models, in the statistical ensemble or individual tomography models, can reconcile the counter-clockwise rotation of Adria with respect to Eurasia; in all cases, surface motion resembles a pattern typical of a dense lithosphere sinking into a surrounding buoyant asthenosphere (Text S4 and Figures S9–S13 in Supporting Information S1). Although our models reproduce the first-order observations in the Alps and its foreland regions, modeled topography does not match observations in the Adriatic Sea. A possible reason for this mismatch stems from a lack of constraints on the configuration and nature of the crust in this region. It is also possible that the present-day deformation in the Adriatic Sea is influenced significantly by a far-field Mediterranean-scale mantle flow not included in this study (Faccenna & Becker, 2010; Faccenna et al., 2014).

Our models also fail in reproducing the coherent orogen parallel flow in the asthenosphere, inferred as a proxy in the SKS measurements. These discrepancies demand attention to which additional factors could influence this behavior. Return flow from neighboring slabs in the Mediterranean could provide an alternative (e.g., Kiraly et al., 2021). Our models are spatially limited to the Alps and Northern Apennines, and therefore we could not quantify to which degree the present-day mantle flow in the Alps can be affected by such a Mediterranean-scale return flow from the Aegean subduction in the east and W-E directed mantle flow from the west (Faccenna & Becker, 2010).

We finally note that despite modeled vertical velocities in the Alps being of a similar order of magnitudes as for available observations, we could not fully reproduce the details of their along-strike variability, which likely results from a heterogeneous load distribution from long-term erosion, ice-sheet thickness variations, and lithospheric loads. Further work is therefore required to quantify the relative contribution from surface processes and their coupling to the active tectonic processes investigated in this study within higher resolution models.

Data Availability Statement

The crustal models used can be downloaded from Spooner et al., (2019b) (https://doi.org/10.5880/GFZ.4.5.2019.004) and Tesauro et al. (2008) (https://gfzpublic.gfz-potsdam.de/pubman/item/item_238001). Seismic tomography models can be downloaded from http://ds.iris.edu/ds/products/emc-earthmodels/. LaMEM is an open-source code and can be downloaded from https://doi.org/10.5281/zenodo.7071571 or https://bitbucket.org/bkaus/lamem/src/master/. Code used for converting seismic velocities to temperatures can be downloaded from https://doi.org/10.5281/zenodo.6538257 or https://github.com/ajay6763/V2RhoT_gibbs.git. Post-processing and plotting of the results was done using ParaView (Ahrens et al., 2005) (https://www.paraview.org/), GMT5 (Wessel et al., 2013), Matplotlib (Hunter, 2007), and Inkscape (https://inkscape.org/). Scientific color maps from Crameri (2021) were used for visualization.

Acknowledgments
This work is funded by the Deutsche Forschungsgemeinschaft (DFG) through DEFORM project within "Mountain Building Processes in Four Dimensions (4DMB)" SPP (SCHE 674/8-1). The authors acknowledge the Earth System Modelling Project (ESM) by providing computing time on JUWELS cluster, Jülich Supercomputing Centre (JSC) under the application 24312 titled "Unconventional exploration methods for complex tectonic systems-linking geology and geodynamics via numerical model" and GAIA cluster, Johannes Gutenberg University of Mainz. We thank Lucy Flesch for editorial handling and two anonymous reviewers for their comments and suggestions. Open access funding enabled and organized by Projekt DEAL.

References

Afonso, J. C., Fernàndez, M., Ranalli, G., Griffin, W. L., & Connolly, J. A. D. (2008). Integrated geophysical-petrological modeling of the lithosphere and sublithospheric upper mantle: Methodology and applications. *Geochemistry, Geophysics, Geosystems*, *9*(5), Q05008. https://doi.org/10.1029/2007GC001834

Afonso, J. C., Rawlinson, N., Yang, Y., Schutt, D. L., Jones, A. G., Fullea, J., & Griffin, W. L. (2016). 3-D multiobservable probabilistic inversion for the compositional and thermal structure of the lithosphere and upper mantle: III. Thermochemical tomography in the Western-Central U.S. *Journal of Geophysical Research: Solid Earth*, *121*(5), Y7337–Y7370. https://doi.org/10.1002/2016JB013049

Afonso, J. C., & Zlotnik, S. (2011). The subductability of continental lithosphere: The before and after story frontiers in Earth sciences. In *Arc-Continent Collision* (Vol. 4. pp. 53–86). https://doi.org/10.1007/978-3-540-88558-0

Ahrens, J., Geveci, B., & Law, C. (2005). Paraview: An end-user tool for large data visualization Handbook, Elsevier.

Amante, C., & Eakins, B. W. (2009). *ETOPO1 1 arc-minute global relief model: Procedures, data sources and analysis*. NOAA Technical Memorandum NESDIS NGDC-24. https://doi.org/10.1594/PANGAEA.769615

Artemieva, I. M. (2019). Lithosphere structure in Europe from thermal isostasy. *Earth-Science Reviews*, *188*, 454–468. https://doi.org/10.1016/j.earscirev.2018.11.004

Bagagli, M., Molinari, I., Diehl, T., Kissling, E., Giardini, D., & Groupthe, A. W. (2022). The AlpArray Research seismicity-catalogue. *Geophysical Journal International*, ggac226. https://doi.org/10.1093/gji/ggac226

Barruol, G., Bonnin, M., Pedersen, H., Bokelmann, G. H. R., & Tiberi, C. (2011). Belt-parallel mantle flow beneath a halted continental collision: The Western Alps. *Earth and Planetary Science Letters*, *302*(3–4), 429–438. https://doi.org/10.1016/j.epsl.2010.12.040

Boonma, K., Kumar, A., Garcia-Castellanos, D., Jiménez-Munt, I., & Fernández, M. (2019). Lithospheric mantle buoyancy: The role of tectonic convergence and mantle composition. *Scientific Reports*, *9*(1), 1–8. https://doi.org/10.1038/s41598-019-54374-w

Cammarano, F., Goes, S., Vacher, P., & Giardini, D. (2003). Inferring upper-mantle temperatures from seismic velocities. *Physics of the Earth and Planetary Interiors*, *138*(3–4), 197–222. https://doi.org/10.1016/S0031-9201(03)00156-0

Cattaneo, M., Augliera, P., Parolai, S., & Spallarossa, D. (1999). Anomalously deep earthquakes in northwestern Italy. *Journal of Seismology*, *3*(4), 421–435. https://doi.org/10.1023/A:1009899214734

Chiarabba, C., Jovane, L., & DiStefano, R. (2005). A new view of Italian seismicity using 20 years of instrumental recordings. *Tectonophysics*, *395*(3–4), 251–268. https://doi.org/10.1016/j.tecto.2004.09.013

Connolly, J. A. D. (2005). Computation of phase equilibria by linear programming: A tool for geodynamic modeling and its application to subduction zone decarbonation. *Earth and Planetary Science Letters*, *236*(1–2), 524–541. https://doi.org/10.1016/j.epsl.2005.04.033

Connolly, J. A. D. (2009). The geodynamic equation of state: What and how. *Geochemistry, Geophysics, Geosystems*, *10*(10), Q10014. https://doi.org/10.1029/2009GC002540

Crameri, F. (2021). Scientific colour maps (Version 7.0.1) [Computer software]. Zenodo. https://doi.org/10.5281/ZENODO.5501399

Crameri, F., Schmeling, H., Golabek, G. J., Duretz, T., Orendt, R., Buiter, S. J. H., et al. (2012). A comparison of numerical surface topography calculations in geodynamic modelling: An evaluation of the "sticky air" method. *Geophysical Journal International*, *189*(1), 38–54. https://doi.org/10.1111/j.1365-246X.2012.05388.x

Dal Zilio, L., van Dinther, Y., Gerya, T. V., & Pranger, C. C. (2018). Seismic behaviour of mountain belts controlled by plate convergence rate. *Earth and Planetary Science Letters*, *482*, 81–92. https://doi.org/10.1016/j.epsl.2017.10.053

Deichmann, N. (1992). Structural and rheological implications of lower-crustal earthquakes below northern Switzerland. *Physics of the Earth and Planetary Interiors*, *69*(3–4), 270–280. https://doi.org/10.1016/0031-9201(92)90146-M

El-Sharkawy, A., Meier, T., Lebedev, S., Behrmann, J. H., Hamada, M., Cristiano, L., et al. (2020). The slab puzzle of the Alpine-Mediterranean region: Insights from a new, high-resolution, shear wave velocity model of the upper mantle. *Geochemistry, Geophysics, Geosystems*, *21*(8), e2020GC008993. https://doi.org/10.1029/2020GC008993

Eva, E., Malusà, M. G., & Solarino, S. (2015). A seismotectonic picture of the inner southern Western Alps based on the analysis of anomalously deep earthquakes. *Tectonophysics*, *661*, 190–199. https://doi.org/10.1016/j.tecto.2015.08.040

Faccenna, C., & Becker, T. W. (2010). Shaping mobile belts by small-scale convection. *Nature*, *465*(7298), 602–605. https://doi.org/10.1038/nature09064

Faccenna, C., Becker, T. W., Auer, L., Billi, A., Boschi, L., Brun, J. P., et al. (2014). Mantle dynamics in the Mediterranean. *Reviews of Geophysics*, *52*(3), 283–332. https://doi.org/10.1002/2013RG000444

Fernández-García, C., Guillaume, B., & Brun, J. P. (2019). 3D slab breakoff in laboratory experiments. *Tectonophysics*, *773*, 1–11. https://doi.org/10.1016/j.tecto.2019.228223

Fichtner, A., Trampert, J., Cupillard, P., Saygin, E., Taymaz, T., Capdeville, Y., & Villaseñor, A. (2013). Multiscale full waveform inversion. *Geophysical Journal International*, *194*(1), 534–556. https://doi.org/10.1093/gji/ggt118

Fichtner, A., van Herwaarden, D. P., Afanasiev, M., Simutė, S., Krischer, L., Çubuk-Sabuncu, Y., et al. (2018). The collaborative seismic Earth model: Generation 1. *Geophysical Research Letters*, *45*(9), 4007–4016. https://doi.org/10.1029/2018GL077338

Foulger, G. R., Panza, G. F., Artemieva, I. M., Bastow, I. D., Cammarano, F., Evans, J. R., et al. (2013). Caveats on tomographic images. *Terra Nova*, *25*(4), 259–281. https://doi.org/10.1111/ter.12041

Fox, M., Herman, F., Kissling, E., & Willett, S. D. (2015). Rapid exhumation in the Western Alps driven by slab detachment and glacial erosion. *Geology*, *43*(5), 379–382. https://doi.org/10.1130/G36411.1

Goes, S., Govers, R., & Vacher, P. (2000). Shallow mantle temperatures under Europe from *P* and *S* wave tomography. *Journal of Geophysical Research*, *105*(B5), 11153–11169. https://doi.org/10.1029/1999JB900300

Griffin, W. L., O'Reilly, S. Y., Afonso, J. C., & Begg, G. C. (2009). The Composition and Evolution of Lithospheric Mantle: a Re-evaluation and its Tectonic Implications. *Journal of Petrology*, *50*(7), 1185–1204. https://doi.org/10.1093/petrology/egn033

Hammond, W. C., & Humphreys, E. D. (2000). Upper mantle seismic wave attenuation: Effects of realistic partial melt distribution. *Journal of Geophysical Research*, *105*(B5), 10987–10999. https://doi.org/10.1029/2000jb900042

Handy, M. R., Schmid, S. M., Paffrath, M., & Friederich, W. (2021). Orogenic lithosphere and slabs in the greater Alpine area - interpretations based on teleseismic *P*-wave tomography. *Solid Earth*, *12*(11), 2633–2669. https://doi.org/10.5194/se-12-2633-2021

Hein, G., Kolinsky, P., Bianchi, I., Bokelmann, G., Hetenyi, G., Abreu, R., et al. (2021). Shear wave splitting in the Alpine region. *Geophysical Journal International*, *227*(3), 1996–2015. https://doi.org/10.1093/gji/ggab305

Heit, B., Mancilla, F. L., Yuan, X., Morales, J., Stich, D., Martín, R., & Molina-Aguilera, A. (2017). Tearing of the mantle lithosphere along the intermediate-depth seismicity zone beneath the Gibraltar Arc: The onset of lithospheric delamination. *Geophysical Research Letters*, *44*(9), 4027–4035. https://doi.org/10.1002/2017GL073358

Hirschmann, M. M. (2000). Mantle solidus: Experimental constraints and the effects of peridotite composition. *Geochemistry, Geophysics, Geosystems*, *1*(10), 1042. https://doi.org/10.1029/2000GC000070

Holland, T. J. B., & Powell, R. (1998). An internally consistent thermodynamic data set for phases of petrological interest. *Journal of Metamorphic Geology*, *16*(3), 309–343. https://doi.org/10.1111/j.1525-1314.1998.00140.x

Hunter, J. D. (2007). Matplotlib: A 2D Graphics Environment. *Computing in Science & Engineering*, *9*(3), 90–95. https://doi.org/10.1109/mcse.2007.55

Jackson, I., & Faul, U. H. (2010). Grainsize-sensitive viscoelastic relaxation in olivine: Towards a robust laboratory-based model for seismological application. *Physics of the Earth and Planetary Interiors*, *183*(1–2), 151–163. https://doi.org/10.1016/j.pepi.2010.09.005

Kästle, E. D., Rosenberg, C., Boschi, L., Bellahsen, N., Meier, T., & El-Sharkawy, A. (2020). Slab break-offs in the Alpine subduction zone. *International Journal of Earth Sciences*, *109*(2), 587–603. https://doi.org/10.1007/s00531-020-01821-z

Kaus, B. J. P., Mühlhaus, H., & May, D. A. (2010). A stabilization algorithm for geodynamic numerical simulations with a free surface. *Physics of the Earth and Planetary Interiors*, *181*(1–2), 12–20. https://doi.org/10.1016/j.pepi.2010.04.007

Kennett, B. L. N., & Engdahl, E. R. (1991). Traveltimes for global earthquake location and phase identification. *Geophysical Journal International*, *105*(2), 429–465. https://doi.org/10.1111/j.1365-246x.1991.tb06724.x

Kiraly, A., Funiciello, F., Capitanio, F. A., & Faccenna, C. (2021). Dynamic interactions between subduction zones. *Global and Planetary Change*, *202*, 103501. https://doi.org/10.1016/j.gloplacha.2021.103501

Kissling, E., & Schlunegger, F. (2018). Rollback orogeny model for the evolution of the Swiss Alps. *Tectonics*, *37*(4), 1097–1115. https://doi.org/10.1002/2017TC004762

Kumar, A., Fernàndez, M., Jimenez-Munt, I., Torne, M., Vergés, J., & Afonso, J. C. (2020). LitMod2D_2.0: An improved integrated geophysical-petrological modeling tool for the physical interpretation of upper mantle anomalies. *Geochemistry, Geophysics, Geosystems*, *21*(3), 1–19. https://doi.org/10.1029/2019gc008777

Lippitsch, R., Kissling, E., & Ansorge, J. (2003). Upper mantle structure beneath the Alpine orogen from high-resolution teleseismic tomography. *Journal of Geophysical Research*, *108*(B8), 1–15. https://doi.org/10.1029/2002jb002016

Mancilla, F. d. L., Stich, D., Morales, J., Martín, R., Diaz, J., Pazos, A., et al. (2015). Crustal thickness and images of the lithospheric discontinuities in the Gibraltar arc and surrounding areas. *Geophysical Journal International*, *203*(3), 1804–1820. https://doi.org/10.1093/gji/ggv390

Marotta, A. M., & Splendore, R. (2014). 3D mechanical structure of the lithosphere below the Alps and the role of gravitational body forces in the regional present-day stress field. *Tectonophysics*, *631*, 117–129. https://doi.org/10.1016/j.tecto.2014.04.038

Mey, J., Scherler, D., Wickert, A. D., Egholm, D. L., Tesauro, M., Schildgen, T. F., & Strecker, M. R. (2016). Glacial isostatic uplift of the European Alps. *Nature Communications*, *7*, 1–10. https://doi.org/10.1038/ncomms13382

Paffrath, M., Friederich, W., Schmid, S. M., & Handy, M. R. (2021). Imaging structure and geometry of slabs in the greater Alpine area—A *P*-wave travel-time tomography using AlpArray Seismic Network data. *Solid Earth*, *12*(11), 2671–2702. https://doi.org/10.5194/se-12-2671-2021

Priestley, K., & McKenzie, D. (2006). The thermal structure of the lithosphere from shear wave velocities. *Earth and Planetary Science Letters*, *244*(1–2), 285–301. https://doi.org/10.1016/j.epsl.2006.01.008

Schaeffer, A. J., & Lebedev, S. (2013). Global shear speed structure of the upper mantle and transition zone. *Geophysical Journal International*, *194*(1), 417–449. https://doi.org/10.1093/gji/ggt095

Serpelloni, E., Cavaliere, A., Martelli, L., Pintori, F., Anderlini, L., Borghi, A., et al. (2022). Surface velocities and strain-rates in the Euro-Mediterranean region from massive GPS data processing. *Frontiers of Earth Science*, *10*, 1–21. https://doi.org/10.3389/feart.2022.907897

Serpelloni, E., Vannucci, G., Anderlini, L., & Bennett, R. A. (2016). Kinematics, seismotectonics and seismic potential of the eastern sector of the European Alps from GPS and seismic deformation data. *Tectonophysics*, *688*, 157–181. https://doi.org/10.1016/j.tecto.2016.09.026

Singer, J., Diehl, T., Husen, S., Kissling, E., & Duretz, T. (2014). Alpine lithosphere slab rollback causing lower crustal seismicity in northern foreland. *Earth and Planetary Science Letters*, *397*, 42–56. https://doi.org/10.1016/j.epsl.2014.04.002

Spooner, C., Scheck-Wenderoth, M., Cacace, M., & Anikiev, D. (2022). How Alpine seismicity relates to lithospheric strength. *International Journal of Earth Sciences*, *111*(4), 1–24. https://doi.org/10.1007/s00531-022-02174-5

Spooner, C., Scheck-Wenderoth, M., Cacace, M., Götze, H. J., & Luijendijk, E. (2020). The 3D thermal field across the Alpine orogen and its forelands and the relation to seismicity. *Global and Planetary Change*, *193*, 103288. https://doi.org/10.1016/j.gloplacha.2020.103288

Spooner, C., Scheck-Wenderoth, M., Götze, H.-J., Ebbing, J., & Hetényi, G. (2019a). Density distribution across the Alpine lithosphere constrained by 3D gravity modelling and relation to seismicity and deformation. *Solid Earth Discussions*, *10*, 2073–2088. https://doi.org/10.5194/se-2019-115

Spooner, C., Scheck-Wenderoth, M., Götze, H.-J., Ebbing, J., & Hetényi, G. (2019b). 3D Gravity Constrained Model of Density Distribution Across the Alpine Lithosphere [Data set]. GFZ Data Services. https://doi.org/10.5880/GFZ.4.5.2019.004

Sternai, P., Jolivet, L., Menant, A., Gerya, T., Yakovlev, P. V., Saal, A., et al. (2014). Driving the upper plate surface deformation by slab rollback and mantle flow. *Earth and Planetary Science Letters*, *405*, 110–118. https://doi.org/10.1016/j.epsl.2014.08.023

Sternai, P., Sue, C., Husson, L., Serpelloni, E., Becker, T. W., Willett, S. D., et al. (2019). Present-day uplift of the European Alps: Evaluating mechanisms and models of their relative contributions. *Earth-Science Reviews*, *190*, 589–604. https://doi.org/10.1016/j.earscirev.2019.01.005

Tesauro, M., Kaban, M. K., & Cloetingh, S. A. P. L. (2008). EuCRUST-07: A new reference model for the European crust. *Geophysical Research Letters*, *35*(5), 3–7. https://doi.org/10.1029/2007GL032244

Wenzel, F., Sperner, B., Lorenz, F., & Mocanu, V. (2002). Geodynamics, tomographic images and seismicity of the Vrancea region,). *EGU Stephan Mueller special publication series*, 95–104.

Wessel, P., Smith, W. H. F., Scharroo, R., Luis, J., & Wobbe, F. (2013). Generic Mapping Tools: Improved Version Released. *Transactions American Geophysical Union*, *94*(45), 409–410. https://doi.org/10.1002/2013eo450001

Willingshofer, E., & Cloetingh, S. (2003). Present-day lithospheric strength of the Eastern Alps and its relationship to neotectonics. *Tectonics*, *22*(6), 1075. https://doi.org/10.1029/2002TC001463

Winter, J. D. (2010). *An introduction to igneous and metamorphic petrology*. Prentice Hall.

Workman, R. K., & Hart, S. R. (2005). Major and trace element composition of the depleted MORB mantle (DMM). *Earth and Planetary Science Letters*, *231*(1–2), 53–72. https://doi.org/10.1016/j.epsl.2004.12.005

Zhu, H., Bozdağ, E., & Tromp, J. (2015). Seismic structure of the European upper mantle based on adjoint tomography. *Geophysical Journal International*, *201*(1), 18–52. https://doi.org/10.1093/gji/ggu492